Self-Growing Hydrogel Bioadhesives for Chronic Wound Management

Ziman Zheng, Xingmei Chen, Yafei Wang, Ping Wen, Qingfang Duan, Pei Zhang, Liangjie Shan, Zhipeng Ni, Yinghui Feng, Yu Xue, Xing Li, Lin Zhang,* and Ji Liu*

Hydrogel bioadhesives have emerged as a promising alternative to wound dressings for chronic wound management. However, many existing bioadhesives do not meet the functional requirements for efficient wound management through dynamically mechanical modulation, due to the reduced wound contractibility, frequent wound recurrence, incapability to actively adapt to external microenvironment variation, especially for those gradually-expanded chronic wounds. Here, a self-growing hydrogel bioadhesive (sGHB) patch that exhibits instant adhesion to biological tissues but also a gradual increase in mechanical strength and interfacial adhesive strength within a 120-h application is presented. The gradually increased mechanics of the sGHB patch could effectively mitigate the stress concentration at the wound edge, and also resist the wound expansion at various stages, thus mechanically contracting the chronic wounds in a programmable manner. The self-growing hydrogel patch demonstrated enhanced wound healing efficacy in a mouse diabetic wound model, by regulating the inflammatory response, promoting the faster re-epithelialization and angiogenesis through mechanical modulation. Such kind of self-growing hydrogel bioadhesives have potential clinical utility for a variety of wound management where dynamic mechanical modulation is indispensable.

1. Introduction

The wound healing process involves three crucial stages, inflammation, proliferation, and remodeling, aligned in a progressive and orderly manner.[1] For chronic wounds, such as diabetic foot ulcer, the disrupted immune microenvironments, i.e., macrophage dysfunction, cause excessive inflammatory response, thus disorganizing the wound-healing process or even leading to non-healable wounds.[2,3] In the past decade, tremendous efforts have been dedicated to biomaterials-based management of chronic wounds, particularly using hydrogels,[4–6] in light of their unique capabilities, including maintaining a wet and soft environment, offering a mechanically compliant interface, and also encapsulation of various bioactive components (i.e., biomolecules, therapeutics, cells).[5,6] However, as a passive and protective wound dressing strategy, the therapeutic efficacy of conventional hydrogels for wound management is limited, associated with reduced wound contractibility, frequent wound recurrence, incapability to actively adapt to external microenvironment variation, especially for those gradually-expanded chronic wounds.[5,7,8] Thus, there remains a long-lasting clinical desire for more effective approaches to address this crucial challenge in chronic wound management.
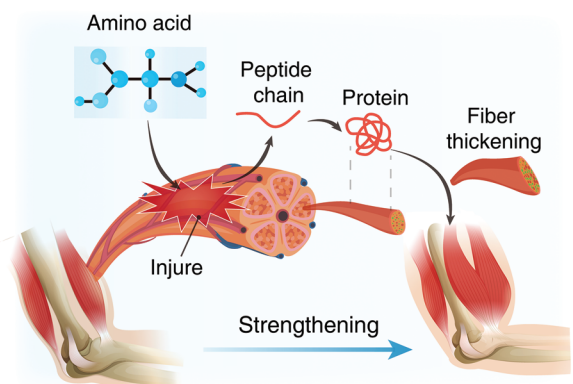
Mechanical modulation has emerged as an attractive approach for chronic wound management, by enhancing the granulation tissue formation, wound contraction, and epithelialization.[7,9] However, variations exist in the mechanical forces and cellular processes involved in each stage of wound healing.[10,11] Notably, the late stage of wound healing features dramatically stronger traction forces against the wound closure compared to the early stage.[12] Moreover, excessive extrinsic mechanical loading can accelerate angiogenesis, cell proliferation, and collagen hyperproduction, ultimately leading to abnormal scar formation.[11,13,14] Despite recent advancements in hydrogel bioadhesives for chronic wound management,[4,7,8] most of them failed to provide dynamically mechanical modulation by adapting to each stage of the wound healing. This could be ascribed to the static mechanical modulation, not to mention the gradually deteriorated mechanical contraction caused by wound exudates infiltration, stress relaxation, and hydrogel network destruction

Z. Zheng, X. Chen, Y. Wang, P. Wen, Q. Duan, P. Zhang, L. Shan, Z. Ni,
Y. Feng, Y. Xue, J. Liu
Department of Mechanical and Energy Engineering
Southern University of Science and Technology
Shenzhen 518055, China
E-mail: liuj9@sustech.edu.cn
Z. Zheng, L. Zhang
Engineering Research Center for Nanomaterials
Henan University
Kaifeng 475004, China
E-mail: lin.zhang@henu.edu.cn
X. Li
Department of Medical Neuroscience
School of Medicine
Southern University of Science and Technology
Shenzhen 518055, China
J. Liu
Shenzhen Key Laboratory of Intelligent Robotics and Flexible
Manufacturing Systems
Southern University of Science and Technology
Shenzhen 518055, China
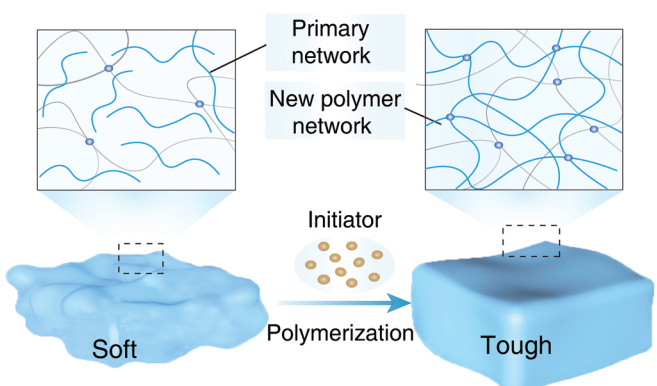
Figure 1. Self-growing hydrogel bioadhesives (sGHB) for wound management. a). Schematic illustration for wound management with the assistance of a hydrogel patch. i). Compared with traditional hydrogel patch, the unique gradually-strengthening attribute of our sGHB could effectively alleviate residual stress, resist the wound expansion and facilitate the wound healing. Difference in the evolution of applied stress ii) and wound size iii) when our proposed sGHB patch is applied, compared with conventional wound dressing patches. b). Schematic illustration for the in situ muscle growing through the formation of extra muscle fibers from nutrient supplies within the metabolic cycles. c). Self-growing mechanism of the sGHB. The endogenous replenishment (e.g., glucose) initiates the polymerization of a new polymer network, accompanied by a gradual strengthening in mechanics from a soft to a strong hydrogel.

(**Figure 1a**), thus leading to ineffective and uncontrolled wound contraction, and/or partially cured wounds in a passive manner. To the best of our knowledge, there exists no strategy that can provide long-term yet dynamic mechanical modulation over chronic wounds, leaving this promising strategy untapped for chronic wound management.

Herein, inspired by the self-growing behavior and mechanism of biological tissues (i.e., muscle, Figure 1b), we reported a self-growing hydrogel bioadhesives (sGHB) patch, offering precisely and dynamically programmed mechanical modulation for chronic wound management (Figure 1c). Our sGHB patch synergistically combines a dry-crosslinking mechanism and glucose-activated self-growing characteristic, enabling not only a mechanically-robust biointerface, but also a gradually-enhanced bioadhesion interface. The mechanically-adaptive biointerface could provide dynamically mechanical modulation of the dy-

namic wounds, such as mitigating the stress concentration at the wound edge, resisting the wound expansion (Figure 1a), regulating the inflammatory response, and promoting angiogenesis, thus accelerating the healing of chronic wounds. The improved therapeutic efficacy of our sGHB patch has also been validated on chronic wound management, on the basis of diabetic wounds in mouse models. We believe that dynamic mechanical modulation by exploiting the self-growing hydrogel patches would represent the next generation strategy for chronic wound management.

2. Results and Discussion

2.1. Design and Fabrication of the sGHB Patch

We developed a glucose-activated self-growing hydrogel bioadhesive (sGHB) patch with gradually-strengthened mechanical

2408538 (2 of 11)
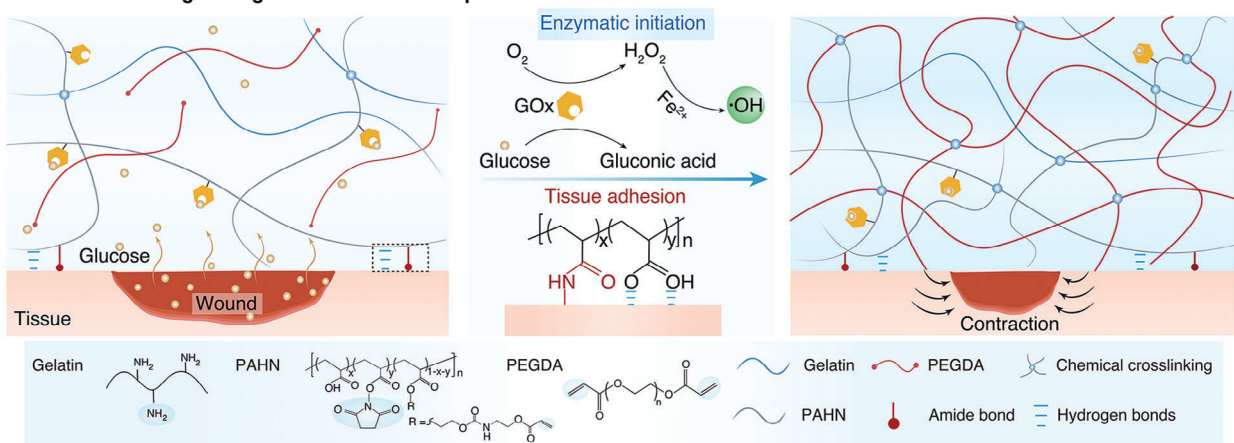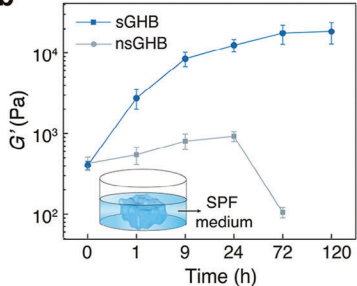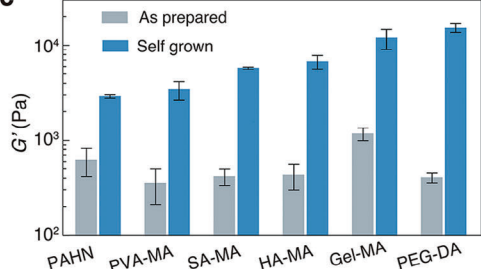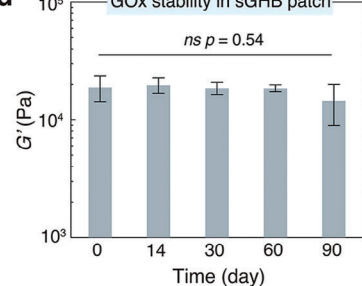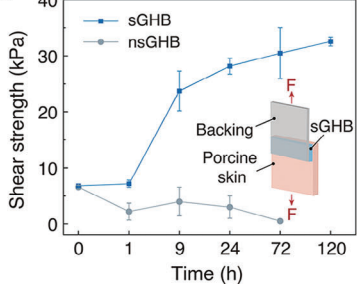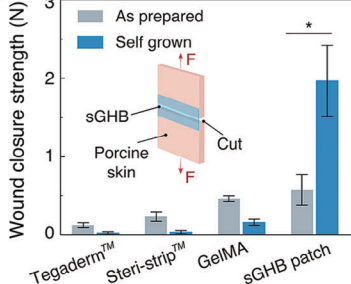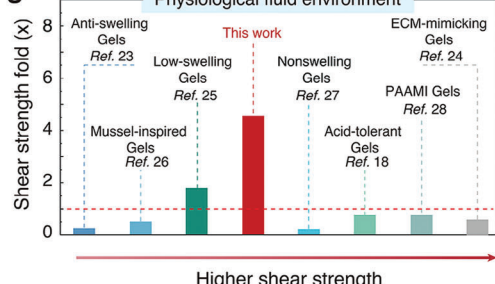
Figure 2. Gradually-enhanced mechanics of the sGHB patches. a). Schematic illustration for the mechanical strengthening mechanism of the sGHB patches through self-growing during the application to a wound. The primary crosslinking of the hydrogel network is established via an amidation reaction between the PAHN and gelatin polymer chains, while the bioadhesion was achieved through the synergistic contribution from amide bonds between NHS (sGHB) and amine moieties (biological tissues) and interfacial hydrogen bonds. Once the sGHB patch is applied to a wound, glucose molecules immediately diffuse into the sGHB hydrogel network, react with GOx and generate radicals, thus initiating the polymerization among the PAHN and PEGDA chains. b). Evolution of the storage modulus (G') of the sGHB within SPF buffer (3 mM glucose in PBS buffer) during 120 h, while a hydrogel patch fabricated using the same formulation as the sGHB patch, but without incorporating GOx, serving as a control (termed nsGHB). c). Summary of mechanical strengthening performance for the sGHB patches made of various acrylate-functionalized polymers, including PVA-MA, SA-MA, HA-MA, Gel-MA and PEGDA. d). sGHB patches in the dehydrated state were stored under −20 °C for various periods, followed by 120-h self growing in SPF, and the final G' values were recorded. e). Evolution of interfacial shear strength for the adhered joints between sGHB patch and porcine skins, during a 120-h soaking within SPF buffers at 37 °C for various periods of time. f). Wound closure strength between our sGHB patch and various tissue bioadhesives before and after 24-h incubation in SPF. g). Comparison chart of the bioadhesion performance of our sGHB patch with previously-reported hydrogel bioadhesives in physiological environments. Data in (b–f) are presented as means ± S.D., $n = 3$.

performance under physiological conditions. As illustrated in **Figure 2a**, the primary network of sGHB consisted of poly(acrylic acid-*co*-hydroxyethyl methacrylate-*co*-*N*-hydroxysuccinimid ester) (PAHN) and gelatin, while covalent and physical crosslinks formed the network structure. Additionally, poly(ethylene glycol) diacrylate (PEGDA, 700 Da), glucose oxidase (GOx), and ferrous ions (Fe^{2+}) were incorporated within the primary network,

while endogenous replenishment, such as glucose molecules, could effectively trigger the chemical crosslinking and gradual increase in mechanics in a self-growing manner.[15,16] In the dehydrate state, the sGHB patch maintained the form of a thin and flexible film (Figure S1, Supporting Information), allowing for direct application onto wet tissues. Upon direct contact, the sGHB patch rapidly adhered onto wet tissues through a dry

crosslinking mechanism, with a robust interface facilitated by the synergistic contribution from both amide bond formation (NHS moieties from PAHN and amine moieties from biological tissues) and interfacial hydrogen bonds (Figure 2a).[17–19] With glucose molecules gradually diffused into the sGHB patch, they immediately reacted with GOx, generated H_2O_2, which further reacted with Fe^{2+} ions and formed ·OH radicals through a Fenton-like reaction,[20] and then initiated the polymerization among PAHN and PEGDA chains. Therefore, the sGHB could be gradually strengthened in vivo in an autonomous and self-growing manner, enabling the hydrogel patch to resist the wound traction forces. Importantly, similarly to our previous work,[21] GOx is covalently bonded to the PHAN chain through the formation of amide bonds, effectively preventing the leakage of enzymes from the hydrogel networks (Figure S2, Supporting Information). As a control, we prepared hydrogel patch of the same formulation, but without GOx (termed as nsGHB), and also tested the evolution in mechanics for comparison.

As depicted in Figure 2b and Figures S3 and S4 (Supporting Information), upon soaking into a PBS buffer supplemented with 3 mM glucose (simulated physiological fluid, SPF) at 37 °C for 72 h, the storage modulus (G') of the sGHB patch gradually increased by 45 folds. The enzyme-catalyzed crosslinking kinetics of the sGHB patch could also be tracked using FTIR analysis. As shown in Figure S5 (Supporting Information), the peak at 1550 cm^{-1}, corresponding to the symmetrical stretching vibration of the acrylate moieties (C =C bonds), nearly disappeared after soaking in SPF buffer for 72 h, indicating the This indicates the completion of the second crosslinking within the sGHB patches. The sGHB patch reached its equilibrium state in 72 h, maintaining a substantial water content of ca. 60% and swelling ratio of 300%, respectively (Figures S6 and S7, Supporting Information). Interestingly, for the control group in the absence of glucose, a slight increase in G' (from 0.4 to 0.9 kPa) occurred in the initial 24 h, attributing to the cross-linking among PHAN and gelatin chains (Figures S8 and S9, Supporting Information); afterward, G' gradually decreased by 10 folds within 72 h, due to the uncontrolled volumetric swelling. Additionally, the self-growing behavior was also validated by the enhancement in other mechanical attributes (e.g., tensile strength, Young's modulus, and compression strength) during a 72-h soaking within SPF buffer (Figures S10–S12 and Table S1, Supporting Information). It also deserves to be mentioned that our design rationale could also be applied to other hydrogel formulation using acrylate-functionlized biopolymers, such as methacrylate-modified polyvinyl alcohol (PVA-MA), sodium alginate (SA-MA), hyaluronic acid (HA-MA) and gelatin (Gel-MA) (Figure 2c). Since the sGHB patches were stored in the dehydrated state, they still retained the growing characters despite a 90-day storage at –20 °C, as evidenced by the FTIR analysis (Figure S13, Supporting Information) and mechanical enhancement validation (Figure 2d).

2.2. Bioadhesion Performance

To quantitatively evaluate the bioadhesion performance, we characterized the interfacial shear strength and wound closure strength with our sGHB patches ex vivo applied to porcine skins (Figure 2e,f; Figure S14, Supporting Information). In addition

the robust interfacial adhesion (shear strength of ca. 6.5 kPa), the adhered interface also experienced a 5-fold enhancement in interfacial shear strength after 72-h soaking in SPF buffer, while over 13-fold decrease was detected for the control group (Figure 2e). This enhanced bioadhesion performance could be attributed to the glucose-triggered mechanical reinforcement of the sGHB patch, which effectively contributed to the increased cohesive role of the hydrogel in the adhered joints. Moreover, the wound closure strength of the sGHB patch reached as high as 2 N on wet tissues after 24-h soaking in SPF buffer (Figure 2f), outperforming those commercially available wound dressings (i.e., Tegaderm and Steri-strip), and widely-used hydrogel bioadhesives (i.e., Gel-MA).

Hydrogel bioadhesives are expected to maintain the efficacy over prolonged periods at the wet tissue interface, yet they often experience undesirable swelling as biological extrudes gradually infiltrates within the network, resulting in a gradual decline in strength and interfacial robustness, thereby limiting their practical applications.[18,22] In Figure 2g and Figure S15 (Supporting Information), we compared the bioadhesion performance of our sGHB patch with both commercially-available wound dressings and previously-reported swelling-resistant hydrogel bioadhesives.[18,23–28] It is evidenced that most hydrogel bioadhesives (i.e., Tegaderm and Steri-strip) typically exhibited lower shear strength in their equilibrium state compared to their initial state (shear strength decreased by 1 to 7 times). Despite various strategies reported to impart hydrogel materials with anti-swelling performance, such as increasing cross-linking density and adjusting polymer-water interactions,[18,23] rarely few systems exhibit gradually strengthening behaviors, for example, a tannic acid-composited Pluronic F127 hydrogel bioadhesive with low-swelling and high-toughness properties displayed a moderate increase in shear strength, improving by 1.8-fold.[25] Remarkably, our sGHB patch exhibited a significant increase in shear strength of ca. 5 folds after 120-h soaking in SPF. Moreover, in vitro cell culture tests corroborated the superior cytocompatability of our sGHB patches through the CCK-8 cell viability (Figure S16a, Supporting Information) and live/dead staining images (Figure S16b, Supporting Information). Therefore, the distinct self growing behavior offers promising applicability in chronic wound management through dynamic mechanical modulation, especially for those hard-to-heal chronic wounds, such as diabetic foot ulcers.

2.3. Mechanical Modulation of Expanded Wound

To validate the capability of our sGHB patch in applying glucose-triggered reinforced mechanics to counteract the residual stress at the wound edges, we conducted an experiment on a circular defect of an artificial skin model, which was prepared from PAAm/gelatin hydrogel (see Experimental part for details).[17] Hydrogel patches were adhered onto the models, and then immersed in SPF buffer, while swelling-induced volumetric expansion of the artificial skin defects was exploited to simulate the gradually-expanded wound (**Figure 3a**). In the absence of any hydrogel patches, the defect experienced an area expansion of 100% ± 6% during a 24-h soaking in SPF buffer at 37 °C. For the hydrogel patches made of nsGHB or ContGel,

**ADVANCED
SCIENCE NEWS**

www.advancedsciencenews.com

**ADVANCED
MATERIALS**

www.advmat.de
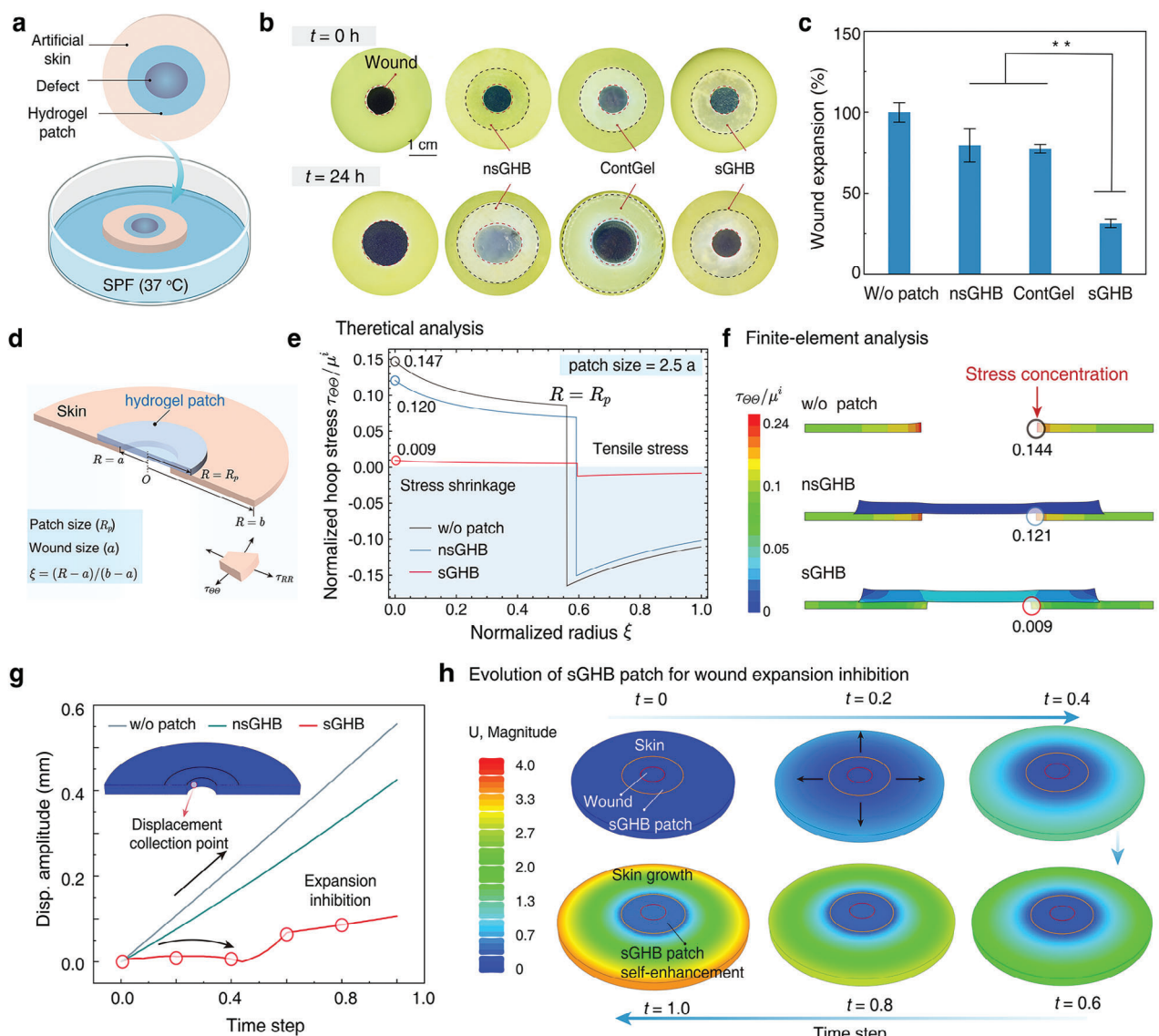
Figure 3. sGHB patches mitigate the dynamic wound expansion. a). Schematic illustration of the sGHB patch for dynamic wound closure. A 1-cm defect of the artificial skin (gelatin/PAAM hydrogel) was sealed with various hydrogel bioadhesives and then soaked within a SPF medium to mimic the aggravated wound expansion. b). Images recording the evolution of sealed defects during a 24-h soaking in SPF medium. Our sGHB patch dramatically inhibits dynamic wound expansion thanks to the self-growing behaviors, while control samples (nsGHB and ContGel) fail due to the uncontrolled swelling of the nsGHB and the incapability of the control samples in resisting the swelling. Scale bar: 1 cm. c). Summary of the wound expansion rate for various hydrogel patches. Artificial skin wound without treatment was tested as a control (100%). d). Schematic illustration for the theoretical and finite-element analyzes of the sGHB patch for dynamic wound management. e). Finite-element and experimental results for the hoop stress (δ_θ/μ^i) around the sealed defects with sGHB or nsGHB patches. f). Mises stress profiles for the sealed defects upon stress loading and the lateral cross-section diagram. g,h). Chart of wound displacement during simulated time step growth of skin (g), and snapshots of wound displacement for wound sealed with sGHB patch (h). Data in (c) is means ± S.D., $n = 3$.

despite their superior bioadhesion performance at the initial state, gradual swelling-induced deterioration of mechanics in both the bulk hydrogel and biointeface was accompanied by a dramatic increase in the wound defects (Figure 3b; Figure S17 and movie S1, Supporting Information). Thanks to the self-growing attribute of our sGHB patch, the wound expansion is efficiently inhibited below 30%, substantially lower than the nsGHB patch (79% ± 10%) and ContGel (77% ± 2.5%) controls (Figure 3b,c).

We subsequently employed nonlinear elasticity theory and finite element analysis to elucidate the underlying physical mechanisms responsible for mechanical modulation in our self-growing hydrogel bioadhesives. As illustrated in Figure 3d, we considered the hydrogel-skin system as a hyperelastic bilayer containing initial residual stress, while the wound radius was set as $R = a$, radius of the skin model as $R = b$, and the hydrogel patch as $R = R_p$. The strain energy function was characterized using the neo-Hookean model $\Psi = \mu^i(\mathbf{C}: \mathbf{I} - 3)/2$, where μ^i represents the

**ADVANCED
SCIENCE NEWS**

www.advancedsciencenews.com

**ADVANCED
MATERIALS**

www.advmat.de

initial shear modulus of the patch or skin, **C** as the right Cauchy–Green tensor, and **I** as the identity tensor.[29] Without loss of generality, we defined a normalized radius $\xi = (R - a)/(b - a) \in [0, 1]$ to describe the entire system. To capture the nonlinear kinematics evolution of the hyperelastic bilayer, we introduced two states: the initial residual stress state and the stress-free state (see Supporting Information for more details).[30,31] The evolution between these two states was governed by the initial stress tensor **S** (and **S**$^{-1}$). The stress τ corresponding to the initial residual stress state can be expressed as:

$$\tau = \mu^i \mathbf{B}_0^{(-1)} - q_0 \mathbf{I} \tag{1}$$

where $\mathbf{B}_0^{(-1)} = \mathbf{S}^{-1}\mathbf{S}^{-T}$, and q_0 is the Lagrangian multiplier (see Supporting Information for more details).

We then theoretically predicted the effect of three different patches (w/o, nsGHB, sGHB patches) on wound stress concentration during a 120-h application. According to Equation 1, Figure 3e depicted the evolution of normalized hoop stress as a function of ξ under three distinct scenarios. It is evident that the pristine skin wound exhibited the highest stress with a peak stress of 0.147 at the wound edges, in the absence of any patches. Upon the application of hydrogel patches, the concentrated stress was reduced to 0.120 for the nsGHB patch. Significantly, the sGHB patch group demonstrated stress at a markedly reduced magnitude (concentrated stress of 0.009), which is two orders of magnitude lower than that observed in the nsGHB scenario, attributable to the spontaneous enhancement of mechanics facilitated by self-growth. Similarly, finite element simulation results corroborated the lowest concentrated stress of 0.009 for the sGHB patch group, substantially lower than the w/o patch (0.144) and nsGHB (0.121) groups (Figure 3f; Figure S18, Supporting Information).

To precisely delineate the evolutionary process, which includes the healing of skin wounds as well as the self-growth and self-reinforcement effects of the sGHB patch, we further implemented nonlinear finite element simulationsbased on volumetric growth theory applied to the hydrogel-skin system with various patches (Figure 3g). A reference point was designated at the wound site, and we charted the trajectory of displacement amplitude at this point across simulation time steps. The displacement amplitude curves for both the scenarios without a patch or with an nsGHB patch (including even the strong hydrogel patch, see Figure S19, Supporting Information) exhibited a linear upward progression. In contrast, the sGHB patch, endowed with self-reinforcement capabilities, significantly mitigated the wound expansion. For the strong hydrogel patch, the parameters of the Arruda–Boyce model are constant, hence they failed to meet the adaptive requirements of the wound during the healing process, corroborating the necessity for a self-growing hydrogel for dynamical mechanical modulation.

The corresponding displacement initially stabilized, then ascended gradually, and eventually leveled off at a significantly lower amplitude. This distinct nonlinear evolutionary pattern, divergent from the other two scenarios, imparted the system with improved strain energy distribution through the self-growing and self-reinforcement mechanisms of the sGHB patch, thus effectively inhibiting the wound expansion and accelerating the wound repairing. Particularly, snapshots under the

sGHB patch condition clearly showed that as the wound expanded, the mechanical modulation through self-growing and self-reinforcement became progressively apparent (Figure 3h; Figures S20,21 and movie S2, Supporting Information). Although the displacement amplitude in the far field of the skin wound continued to increase, the amplitude at the wound site remains consistently unchanged, indicating less residual stress accumulated at the wound edges.

2.4. Wound Healing Efficacy in Chronic Diabetic Mouse Model

A key challenge in treating chronic diabetic wounds is the high-glucose exudate environment (0.65–2.56 mM),[32] which induces M1 macrophage polarization, impairs keratinocyte migration and then promotes glycation to cause a series of side effects, including the reduced wound contractibility, frequent wound recurrence and unexpected wound expansion.[2,33] Our sGHB patch, engineered with glucose-induced mechanical strengthening, holds great promise for chronic wound healing by gradually inhibiting the wound expansion. To evaluate its efficacy, we used streptozotocin (STZ) to establish a chronic diabetic model in mouse (Figure S22, Supporting Information). sGHB patch was applied to a 6-mm dorsal wound, while nsGHB patch and a commercially available wound dressing (Tegaderm) were tested as controls (n = 10, **Figure 4a**; Figure S23 and movie S3, Supporting Information). Subsequently, tissues were sampled on Day 5 and 10 post-injury for histological analysis, and wound healing efficacy was evaluated according to the relative expression of wound biomarkers.

As depicted in Figure 4c,d, diabetic wounds in the Tegaderm group experienced significant expansion (140%±15%) on Day 2, indicating a deterioration under the synergistic effects from residual stress and hyperglycemic exudates. It has been widely established that hydrogel bioadhesives could improve wound healing by absorbing the wound exudates, eliminating bacterial contaminations, and regulating the immune microenvironment.[4–6] The nsGHB patch group did not exhibit obvious expansion owing to the physical barrier and biological fluids absorption in the first two days (Figure 4d). However, due to the inferior mechanical modulation, the wound healing process was significantly slow, and the wound was not completely closed during our 10-day observation (Figure 4c). Interestingly, after 2-day application, G' of the sGHB patch increased by over 10 folds compared to its initial state (Figure 4b; Figure S24 and movie S4, Supporting Information), in accordance with the self growing behaviors we have observed in vitro (Figure 2b). Wound contraction reached over $70 \pm 6\%$ on Day 5 (Figure 4d), significantly outperforming the other control groups, including the Tegaderm group $100 \pm 20\%$) and nsGHB patch ($44 \pm 8\%$).

Histological analysis of full-thickness skin wounds using Masson staining and hematoxylin and eosin staining (H&E) was further performed to assess the effect of sGHB patch on chronic diabetic wound management (Figure 4e; Figure S25, Supporting Information). Masson staining revealed significantly higher collagen deposition and re-epithelialization in the sGHB patch-treated group, compared to the control groups on Day 5 and 10 (Figure 4e). Remarkably, mice treated with the sGHB patch achieved $\approx 67 \pm 6\%$ re-epithelialization on Day 5, whereas
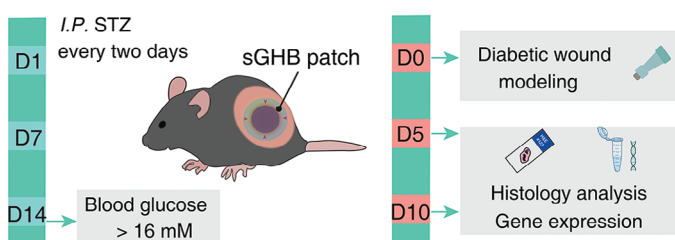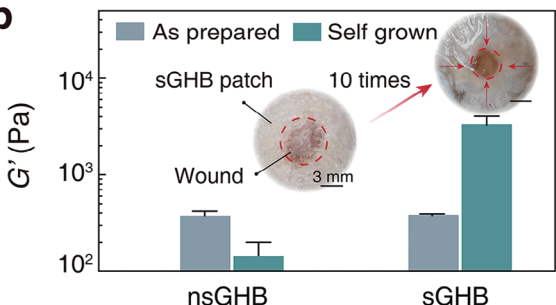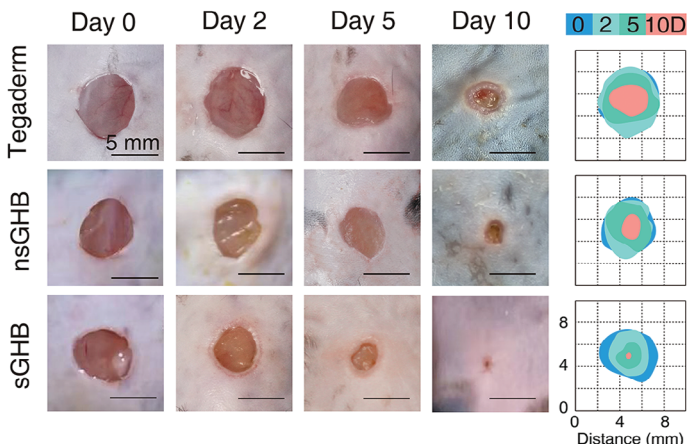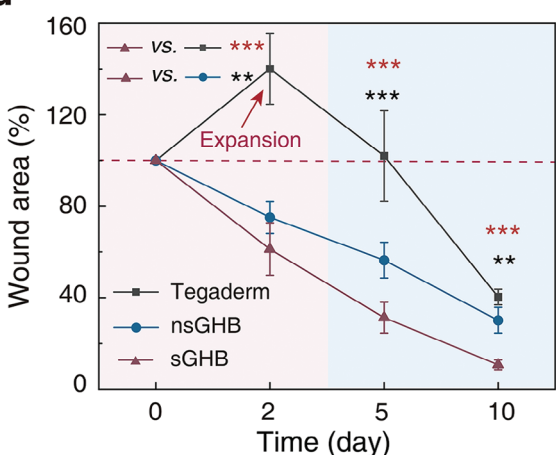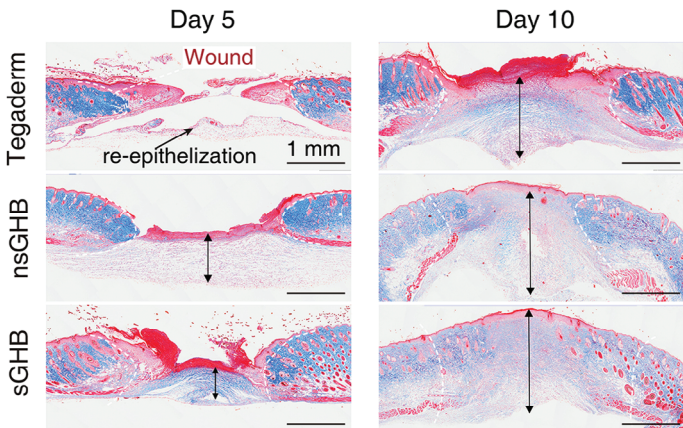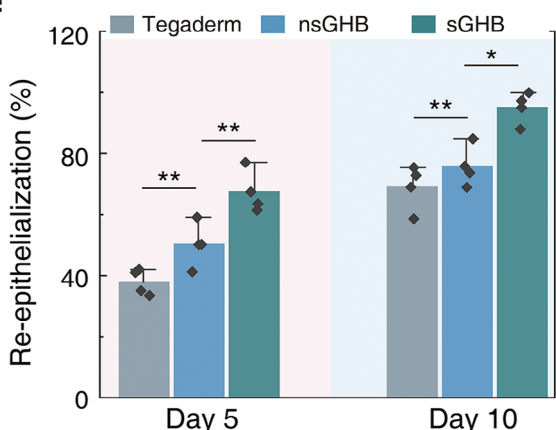
Figure 4. sGHB patches for wound management in diabetic mice. a). Schematic illustration of the timeline for animal experiments to assess the therapeutic effect of sGHB patches in diabetic wound management. b). Summary of G' for the sGHB patches before and after 48-h applying onto diabetic wounds. The diabetic wounds feature high glucose levels, which initiate the self-growing and enhance the mechanics of sGHB patches. Insets are images of diabetic wounds after 48-h treatment with sGHB patches. Scale bar: 3 mm. c,d). Representative images (c) and quantitative analysis (d) of the wound closure upon 10-day treatment with sGHB patches, while Tegaderm and nsGHB patches were tested as controls. Scale bar: 5 mm. Note: for a better visual effect, we removed the hydrogel patches before the images were taken, thus details regarding the wound edge and inflammatory response could be clearly visualized. e). Representative Masson staining images of the full-thickness diabetic wounds after 5 and 10-day treatment, and black arrows indicate the re-epithelializatio thickness. f). Quantification of wound re-epithelialization on Day 5 and 10, as expressed as%, where 100% represents a completely healed wound. Data are presented as means ± S.D. ($n = 4$). Statistical significance was calculated through the one-way ANOVA, *$p < 0.05$, **$p < 0.01$, ***$p < 0.001$.

Tegaderm-treated mice required more than 10 days to reach similar level (69 ± 7%, Figure 4f), corroborating the crucial role of self-growing performance in mechanical modulation of chronic wounds. We also investigated whether the presence of GOx (2 µM) could induce an acute inflammatory response after catalyzing free radical polymerization,[34] by systematically analyzing

white blood cell (WBC), lymphocyte (Lym), and neutrophil (Neu) counts in peripheral blood (Figure S26, Supporting Information). No notable difference in inflammatory cells was detected between mice after 10-day treatment with sGHB patch and healthy mice, excluding the risks of systemic infection and inflammation associated with GOx-loaded hydrogels.[33]

**ADVANCED
SCIENCE NEWS**

www.advancedsciencenews.com

**ADVANCED
MATERIALS**

www.advmat.de

2.5. Molecular Mechanism on Promoting Diabetic Wound Healing

We further explored the molecular mechanisms underlying the application of sGHB patch in chronic wound management through immunocytochemical analysis and quantitative real-time polymerase chain reaction (qPCR) analysis. Revascularization is a crucial part of the wound healing process, and the application time/period and magnitude of mechanical loading directly dominated the microvascular network formation process. For example, a delayed loading (Day 5) significantly upregulated the expression of vascular endothelial growth factor (Vegfa) by 3-fold compared to early loading (Day 0), while a low-magnitude mechanical loading (i.e., 5% strain) effectively promoted early-stage angiogenesis, upregulating Vegfa expression by 2-fold compared to a larger force (30% strain).[11] In our work here, we also investigated the vascular regeneration in the treated tissues using immunofluorescent staining with anti-CD31 (a marker for vascular endothelial cells). As depicted in **Figure 5a,b**, the sGHB patch group exhibited a significantly higher density of CD31$^+$ vessels (27 ± 7 vessels mm^{-2}) on Day 5, compared to those control groups, such as Tegaderm (5 ± 1 vessels mm^{-2}) and nsGHB patch (6 ± 2 vessels mm^{-2}). Moreover, the sGHB patch group exhibited significantly faster angiogenesis due to the enhanced mechanical stress applied to the wound compared to nsGHB patch treatment. In consistence with these previous findings,[11] our experimental data also highlights the sGHB patch's ability to promote neovascularization through dynamic mechanical modulation during chronic wound management.

Myofibroblasts are particularly sensitive to mechanical stress in the wound, and their expression of α-smooth muscle actin (α-SMA) enables them to generate substantial contractile forces. This characteristic allows myofibroblasts to actively contribute to wound contraction, particularly during the initial phases of tissue proliferation;[35] whereas, myofibroblast apoptosis gradually reduces the α-SMA expression as the wound healing progressed, thereby preventing excessive collagen fiber contraction and scar tissue formation.[13,36] Figure 5c,d shows that the sGHB group exhibited significantly higher levels of α-SMA$^+$ cells (1627 ± 200 cells mm^{-2}) on Day 5 compared to the other two control groups. On the other hand, the number of α-SMA$^+$ cells on Day 10 decreased, indicating the progression toward a later stage of wound repairing.[36] This indicates that the application of gradually strengthening mechanical loading adapted to the wound healing process, is advantageous for promoting wound healing and reducing scar formation.[37] Conversely, wounds in the Tegaderm group exhibited relatively high expression of α-SMA (1153 ± 24 cells mm^{-2}), comparable to the sGHB patch group on Day 5. This raised concerns regarding potential scar tissue formation in the Tegaderm group, indicating a much longer time needed to complete the wound healing. Meanwhile, sGHB patch group exhibited significantly higher expression of Collagen I and Collagen III on Day 10, which were 1.7 and 2 times, respectively, higher than the nsGHB group (Figures S27 and S28, Supporting Information). These revealed that the sGHB patch effectively regulated the inflammatory and proliferative phases and promoted the remodeling phase of chronic wound closure, thus contributing to a significant acceleration of wound healing.

As widely established, the wound healing process could be modulated through mechanical stress by regulating inflammatory response via neuropeptide release, enhancing the contraction of myofibroblasts, and generating contractile strain to influence microvascular blood flow.[7,11,12] Here, we conducted a screening of genes associated with wound healing to explore the effect of sGHB patch on chronic wound management. Significantly lower expression of proinflammatory cytokines (IL-6 and TNF-α) was detected for the sGHB group Day 5, compared to the Tegaderm group (Figure 5e,f; Figure S29, Supporting Information). Specifically, the expression of IL-6 and TNF-α in the sGHB patch down-regulated by 7% and 97%, respectively, compared to Tegaderm group (Figure 5g). We attribute the reduced inflammatory response to the synergistic effect from both accelerated neuropeptide release via mechanical stress and glucose consumption by GOx.[38] Additionally, the sGHB group showed a higher level of anti-inflammatory cytokines (Mrc-1, IL-10, Arg-1) compared to the two control groups Figure 5f), suggesting that the healing process has transitioned toward the proliferation phase.[33,39] During the wound healing process, M2 macrophages promoted the recovery of regeneration potential via secreting anti-inflammatory mediators and releasing angiogenic and growth factors.[8] Subsequently, we investigated the impact of the sGHB patch on the expression of pro-angiogenic and wound-healing growth factors, particularly on Day 10, which encompassed Vegfa, Vegf, Fgf-2, Col1a, Col3a1, TGFβ1, and Fgf-2 (Figure 5f and Figure 5h–i), especially, the Vegfa and TGFβ1 have demonstrated response typically activated by mechanical tension during wound healing.[10,40] Despite no significant differences in the expression of genes associated with angiogenesis and wound repairing (Vegf, Fgf-2, Fn1, and TGFβ1) between the sGHB and nsGHB groups on Day 5 (Figure 5h–i), it is noteworthy that these biomarkers were notably upregulated on Day 10 for the sGHB group compared to the nsGHB group. This underscored the key role of the gradually-enhanced mechanical properties of our sGHB patch in continuously promoting the repairing of diabetic wounds. Collectively, these findings corroborate that our sGHB patch could provide dynamic mechanical modulation progressively strengthening mechanical modulation over chronic diabetic wounds, thus promoting the wound healing through regulating the inflammatory response, promoting angiogenesis, and enhancing proliferation.

3. Conclusion

In conclusion, we have demonstrated the dynamically mechanical modulation of chronic wound using a self-growing hydrogel bioadhesive (sGHB) patch, where the endogenous replenishment (i.e., glucose molecules), could effectively trigger the chemical crosslinking and gradual increase in mechanics in a self-growing manner. The gradually increased mechanics of the hydrogel patch could effectively alleviate the residual force near the wound edges, thus significantly resisting the wound expansion. The efficacy of sGHB patch in mechanical modulation has also been predicted and validated through theoretical, numerical and experimental analysis and modeling. In vivo validation in chronic diabetic mouse model has evidenced the improved efficacy in wound management, such as 90% wound closure and 95% re-epithelialization by Day 10 post-injury, outperforming
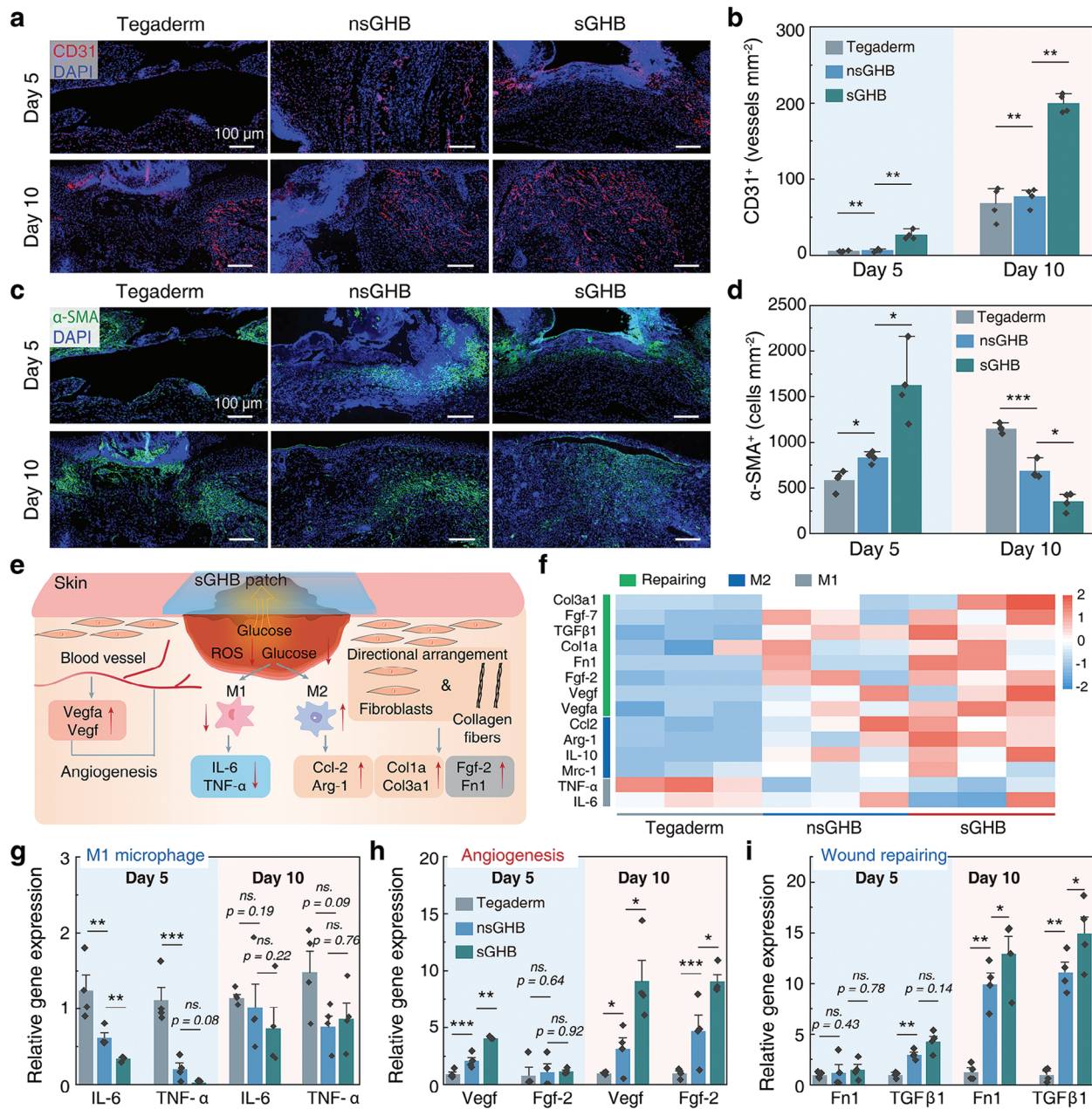
Figure 5. Molecular mechanism for the diabetic wounds healing. a,b). Representative immunofluorescent staining images for vascularization marker CD31(red fluorescence (a), and quantitative analysis of CD31$^+$ vessels per unit area (b) on Day 5 and 10. c,d). Representative immunofluorescent staining images for fibroblast marker α-SMA (green fluorescence (c), and quantitative analysis of α-SMA$^+$ cells per unit area (d) on Day 5 and 10. e). Schematic illustration for wound healing mechanism of sGHB patches, by inhibiting the inflammation, accelerating the angiogenesis, and promoting diabetic wound regeneration. f). Heat map of the upregulated and downregulated genes in the diabetic wound microenvironments after 10-day treatment with different hydrogel patches (sGHB, Tegaderm and nsGHB). (g–i). Relative expression of diabetic wound regeneration biomarkers, including inflammation markers (*IL-6, TNF-α*, (g)), angiogenesis markers (*Vegf, Fgf-2*, (h)) and wound repairing markers (*FN1, TGFβ1*, (i)) after 5 and 10-day treatment. The relative expression data here were presented by normalizing the original qPCR data with reference to the Tegaderm group at the same day. Data are presented as the means ± S.D. (n = 4, (b,d)) or means ± S.E. (n = 4, (g–i)); *p < 0.05, **p < 0.01, ***p < 0.001.

those commercially available wound dressing and other hydrogel bioadhesives. Taking advantage of these distinct capabilities of our sGHB patch, we could envision that our patch technology could provide a versatile platform for easy and cost-effective adaptation toward a broad range of chronic wound management.

4. Experimental Section

Preparation of sGHB patch: The sGHB patch was prepared by incorporating glucose oxidase (GOx) into the crosslinked network made of PAHN and gelatin. Briefly, pre-gel solution A was formulated from an aqueous mixture of 20 *wt*.% PEGDA, 2 μM GOx, and 1.5 mM FeCl$_2$ ·4H$_2$O, along

**ADVANCED
SCIENCE NEWS**

www.advancedsciencenews.com

**ADVANCED
MATERIALS**

www.advmat.de

with 30 *wt*.% gelatin. Pre-gel solution B was comprised of 30 *wt*.% PAHN. The sGHB patch was prepared by mixing an equal volume of pre-gel solution A and B using a double-tube syringe. Subsequently, the resulting mixture was extruded onto a glass mold with a diameter of 10 mm and thickness of 2 mm, followed by air-drying and storage at –20 °C before use. The non-self-growing hydrogel bioadhesive patch (nsGHB) was also prepared by mixing solutions of 30 *wt*.% PAHN and 30 *wt*.% gelatin at a volume ratio of 1:1 using a double-tube syringe, but in the absence of GOx.

In vitro sGHB patches mitigate the expansion of artificial skin defects. To verify the capability of glucose-responsive sGHB patches to inhibit the dynamic expansion of skin wounds, a gelatin/PAAm-based hydrogel with non-controllable swelling was employed to mimic the artificial skin defects. Briefly, a circular notch with a diameter of 1 cm was created in the center of circular gelatin/PAAm hydrogel sample (4 cm in diameter) to simulate the skin wound. The sGHB patch was then applied to seal the defect, and the adhered joints were immersed in SPF medium at 37 °C. During the 24-h soaking within SPF medium, the gelatin/PAAm hydrogels gradually reached the swelling equilibrium, while evolution of circular notches was recorded with a camera. The mitigation rate of wound expansion was determined by quantitatively comparing the size of notches to that of untreated samples (without gel).

$$\text{Wound expansion ratio} = S_{notch}/S_{notch(w/ogel)} \times 100\% \tag{2}$$

Simultaneously, nsGHB patch and ContGels were employed as controls for comparison.

Finite element analysis for stress concentration (FEA):   The finite element analysis (FEA) was employed to assess the mechanical performance and therapeutic effects of the designed self-reinforced hydrogel-based (sGHB) patches on wound healing. Utilizing a 2D axisymmetric model, the complex interaction between the patch and the skin tissue, modeling the latter as an incompressible hyperelastic solid was simplified. Both materials were discretized using a 4-node bilinear axisymmetric quadrilateral element (CAX4RH). The characterization of the skin tissue and its interaction was conducted using cohesive damage properties, incorporating a quadratic stress criterion for damage initiation, which is expressed as follows:

$$\left(\frac{\langle\sigma_n\rangle}{\sigma_n^0}\right)^2 + \left(\frac{\sigma_s}{\sigma_s^0}\right)^2 + \left(\frac{\sigma_t}{\sigma_t^0}\right)^2 = 1 \tag{3}$$

where $\langle\sigma_n\rangle$, σ_s, and σ_t represent the normal and shear stresses, and $\langle\cdot\rangle$ denotes the Macaulay bracket which implies no damage under purely compressive states. The interfacial fracture toughness was further characterized using a power law fracture criterion, taking into account the mixed-mode fracture energies required in different directions:

$$\left(\frac{G_n}{G_n^C}\right)^\alpha + \left(\frac{G_s}{G_s^C}\right)^\alpha + \left(\frac{G_t}{G_t^C}\right)^\alpha = 1 \tag{4}$$

Through simulations in ABAQUS 2019, the mechanical implications of varying patch sizes and the self-reinforcement effect were explored, which was analyzed by adjusting the elastic modulus of the patch. The experiments confirmed that increasing the modulus significantly reduced the hoop stress around the wound, thus validating the effectiveness of the patch design. To accurately depict the evolution of the hyperelastic bilayer under substrate (skin) growth and patch self-reinforcement effects, numerical simulations were conducted using the theory of volumetric growth. These simulations facilitated the decomposition of the overall deformation gradient tensor into an elastic deformation tensor **A** and a growth tensor **G**, specifically expressed as:

$$\mathbf{F} = \mathbf{AG} \tag{5}$$

This approach enabled the analysis of stress distributions and mechanical behaviors in real-time, accommodating the dynamic changes in tissue properties and interactions. Furthermore, the simulations ensured that the stress within the system complied with the balance laws, essential for maintaining equilibrium under evolving conditions. To model this, the following equilibrium condition was used:

$$\nabla \cdot \mathbf{P} = \mathbf{0} \tag{6}$$

where **P** represents the first Piola–Kirchhoff stress tensor, which is critical for describing the mechanics of continuous media in the presence of large deformations.

Theoretical analysis: The kinematic behavior of a hyperelastic bilayer subjected to initial stresses was comprehensively analyzed using a neo-Hookean model to describe the strain energy. This approach utilizes the strain energy function $\Psi = \frac{\mu^i(\mathbf{C}:\mathbf{I}-3)}{2}$, where μ^i represents the initial shear modulus and **C** the right Cauchy–Green deformation tensor. This formulation is fundamental in capturing the nonlinear elastic response of materials under large deformations, typical in biomedical applications such as skin patches. In the context of the study, critical radii (R_i, R_m, R_o) corresponding to the inner, interfacial, and outer boundaries of the bilayer were defined within an initially stressed state. Additionally, a stress-free reference state was established to serve as a baseline for quantifying the residual stresses and their impact on the mechanical behavior of the bilayer. To deepen the understanding, the initial residual stress tensor, referenced earlier (see Equation (1)), was recalculated under the principles of material conservation and minimum energy. This led to an adjusted formulation of the residual stress tensor as a function of the modulus μ^i and a scalar field q_0, reflecting the intrinsic material properties and external loading conditions. The redefined tensor $\mathbf{B}_0^{(-1)}$ was crucial in ensuring the isochoric deformation of the bilayer, a condition essential for maintaining constant volume under deformation. This was mathematically expressed as $\text{Div}(\mu^i\mathbf{B}_0^{(-1)} - q_0\mathbf{I}) = \mathbf{0}$, verifying the theoretical consistency of the model with the physical constraints of incompressibility.

In vivo diabetic mouse skin wound healing test: Diabetic C57BL/6 mice model was produced through the intraperitoneal injection of streptozotocin (STZ, 60 mg kg^{-1}, Sigma, USA) in citrate buffer (pH = 4.5) every two days for a week. Two weeks after the STZ injection, the mice with blood glucose exceeding 16 mM were considered as diabetic. To evaluate the wound healing effect, diabetic C57BL/6 mice were anesthetized, and 6 mm diameter full-thickness skin wounds were created using skin biopsy punches on the shaved and sterilized dorsum. The wounded diabetic mice were then randomly divided into three groups ($n = 10$ per group) and treated with sGHB patch, while those treated with Tegaderm and nsGHB patch served as control groups for comparison. Once the patches were applied for a predesignated time interval (i.e., 5 and 10 days), the wound tissues were sampled for further analysis. Half of the collected tissues were fixed with 4% paraformaldehyde solution and embedded in paraffin for further histological and immunohistochemical analyzes and the remaining half was rinsed with PBS buffer and promptly frozen at –80 °C for subsequent qPCR analysis. The primers of tested gene were listed in Table S2 (Supporting Information).

Statistical Analysis: All the data were processed using Origin 2021 and presented as the means ± standard deviation (S.D.) or the means ± standard error (S.E.). One-way analysis of variance (One-way ANOVA) was used to determine the significance level between multiple groups. For statistical analysis between two groups, the two-sided Student's *t*-test was used. The significance levels were considered as *$p < 0.05$, **$p < 0.01$, ***$p < 0.001$.

Supporting Information

Supporting Information is available from the Wiley Online Library or from the author.

Acknowledgements

Conflict of Interest

The authors declare no conflict of interest.

Data Availability Statement

The data that support the findings of this study are available from the corresponding author upon reasonable request.

Keywords

[1] O. A. Peña, P. Martin, *Nat. Rev. Mol. Cell Biol.* **2024**, 1.
[2] S. A. Eming, T. A. Wynn, P. Martin, *Science* **2017**, *356*, 1026.
[3] M. Kharaziha, A. Baidya, N. Annabi, *Adv. Mater.* **2021**, *33*, 2100176.
[4] J. Hu, T. Wei, H. Zhao, M. Chen, Y. Tan, Z. Ji, Q. Jin, J. Shen, Y. Han, N. Yang, L. Chen, Z. Xiao, H. Zhang, Z. Liu, Q. Chen, *Matter* **2021**, *4*, 2985.
[5] Y. Kang, L. Xu, J. Dong, X. Yuan, J. Ye, Y. Fan, B. Liu, J. Xie, X. Ji, *Nat. Commun.* **2024**, *15*, 1042.
[6] N. Lohmann, L. Schirmer, P. Atallah, E. Wandel, R. A. Ferrer, C. Werner, J. C. Simon, S. Franz, U. Freudenberg, *Sci. Transl. Med.* **2017**, *9*, eaai9044.
[7] G. Theocharidis, H. Yuk, H. Roh, L. Wang, I. Mezghani, J. Wu, A. Kafanas, M. Contreras, B. Sumpio, Z. Li, E. Wang, L. Chen, C. F. Guo, N. Jayaswal, X. L. Katopodi, N. Kalavros, C. S. Nabzdyk, I. S. Vlachos, A. Veves, X. Zhao, *Nat. Biomed. Eng.* **2022**, *6*, 1118.
[8] J. Sun, W. Jia, H. Qi, J. Huo, X. Liao, Y. Xu, J. Wang, Z. Sun, Y. Liu, J. Liu, M. Zhen, C. Wang, C. Bai, *Adv. Mater.* **2024**, *36*, 2312440.
[9] G. Yao, X. Mo, C. Yin, W. Lou, Q. Wang, S. Huang, L. Mao, S. Chen, K. Zhao, T. Pan, L. Huang, Y. Lin, *Sci. Adv.* **2022**, *8*, eabl8379.
[10] K. H. Vining, D. J. Mooney, *Nat. Rev. Mol. Cell Biol.* **2017**, *18*, 728.
[11] M. Ruehle, E. Eastburn, S. LaBelle, L. Krishnan, J. Weiss, J. Boerckel, L. Wood, R. Guldberg, N. Willett, *Sci. Adv.* **2020**, *6*, eabb6351.
[12] A. Brugués, E. Anon, V. Conte, J. H. Veldhuis, M. Gupta, J. Colombelli, J. J. Mu ̃noz, G. W. Brodland, B. Ladoux, X. Trepat, *Nat. Phys.* **2014**, *10*, 683.
[13] S. Mascharak, H. E. DesJardins-Park, M. F. Davitt, M. Griffin, M. R. Borrelli, A. L. Moore, K. Chen, B. Duoto, M. Chinta, D. S. Foster, A.

[14] H. Shen, M. Januszyk, S. H. Kwon, G. Wernig, D. C. Wan H. P. Lorenz, G. C. Gurtner, M. T. Longaker, *Science* **2021**, *372*, eaba2374.
[14] L. A. Barnes, C. D. Marshall, T. Leavitt, M. S. Hu, A. L. Moore, J. G. Gonzalez, M. T. Longaker, G. C. Gurtner, *Adv. Wound Care* **2018**, *7*, 47.
[15] N. Jian, R. Guo, L. Zuo, Y. Sun, Y. Xue, J. Liu, K. Zhang, *Adv. Mater.* **2023**, *35*, 2210609.
[16] X. Xiong, H. Wang, L. Xue, J. Cui, *Angew. Chem. Int. Ed.* **2023**, *62*, e202306565.
[17] K. Zhang, X. Chen, Y. Xue, J. Lin, X. Liang, J. Zhang, J. Zhang, G. Chen, C. Cai, J. Liu, *Adv. Funct. Mater.* **2022**, *32*, 2111465.
[18] X. Chen, J. Zhang, G. Chen, Y. Xue, J. Zhang, X. Liang, I. M. Lei, J. Lin, B. B. Xu, J. Liu, *Adv. Funct. Mater.* **2022**, *32*, 2202285.
[19] J. Lin, X. Chen, P. Zhang, Y. Xue, Y. Feng, Z. Ni, Y. Tao, Y. Wang, J. Liu, *Adv. Mater.* **2024**, *36*, 2400181.
[20] M. Deng, M. Zhang, R. Huang, H. Li, W. Lv, X. Lin, R. Huang, Y. Wang, *Biomaterials* **2022**, *289*, 121790.
[21] G. Chen, X. Liang, P. Zhang, S. Lin, C. Cai, Z. Yu, J. Liu, *Adv. Funct. Mater.* **2022**, *32*, 2113262.
[22] P. Ma, W. Liang, R. Huang, B. Zheng, K. Feng, W. He, Z. Huang, H. Shen, H. Wang, D. Wu, *Adv. Mater.* **2023**, 2305400.
[23] S. Bian, L. Hao, X. Qiu, J. Wu, H. Chang, G.-M. Kuang, S. Zhang, X. Hu, Y. Dai, Z. Zhou, F. Huang, C. Liu, X. Zou, W. Liu, W. W. Lu, H. Pan, X. Zhao, *Adv. Funct. Mater.* **2022**, *32*, 2207741.
[24] J. Wu, Z. Pan, Z.-Y. Zhao, M.-H. Wang, L. Dong, H.-L. Gao, C.-Y. Liu, P. Zhou, L. Chen, C.-J. Shi, Z.-Y. Zhang, C. Yang, S.-H. Yu, D.-H. Zou, *Adv. Mater.* **2022**, *34*, 2200115.
[25] L. Zhang, Y. Zhang, F. Ma, X. Liu, Y. Liu, Y. Cao, R. Pei, *J. Mater. Chem. B* **2022**, *10*, 915.
[26] C. Fan, J. Fu, W. Zhu, D.-A. Wang, *Acta Biomater.* **2016**, *33*, 51.
[27] G. Tian, D. Yang, C. Liang, Y. Liu, J. Chen, Q. Zhao, S. Tang, J. Huang, P. Xu, Z. Liu, D. Qi, *Adv. Mater.* **2023**, *35*, 2212302.
[28] J. Yu, Y. Qin, Y. Yang, X. Zhao, Z. Zhang, Q. Zhang, Y. Su, Y. Zhang, Y. Cheng, *Bioact. Mater.* **2023**, *19*, 703.
[29] C. Liu, Y. Du, K. Li, Y. Zhang, Z. Han, Y. Zhang, S. Qu, C. Lü, *J. Mech.Phys. Solids* **2022**, *169*, 105087.
[30] A. Goriely, *The mathematics and mechanics of biological growth*, vol. *45*, Springer, Berlin, Germany **2017**.
[31] Y. Wang, Y. Du, F. Xu, *J. Mech. Phys. Solids* **2023**, *178*, 105360.
[32] Y. Zhu, J. Zhang, J. Song, J. Yang, Z. Du, W. Zhao, H. Guo, C. Wen, Q. Li, X. Sui, L. Zhang, *Adv. Funct. Mater.* **2020**, *30*, 1905493.
[33] Y. Lu, H. Li, J. Wang, M. Yao, Y. Peng, T. Liu, Z. Li, G. Luo, J. Deng, *Adv. Funct. Mater.* **2021**, *31*, 2105749.
[34] L.-H. Fu, Y.-R. Hu, C. Qi, T. He, S. Jiang, C. Jiang, J. He, J. Qu, J. Lin, P. Huang, *ACS Nano* **2019**, *13*, 13985.
[35] F. Klingberg, B. Hinz, E. S. White, *J. Pathol.* **2013**, *229*, 298.
[36] M. V. Plikus, C. F. Guerrero-Juarez, M. Ito, Y. R. Li, P. H. Dedhia, Y. Zheng, M. Shao, D. L. Gay, R. Ramos, T.-C. Hsi, J. W. Oh, X. Wang, A. Ramirez, S. E. Konopelski, A. Elzein, A. Wang, R. J. Supapannachart, H.-L. Lee, C. H. Lim, A. Nace, A. Guo, E. Treffeisen, T. Andl, R. N. Ramirez, R. Murad, S. Offermanns, D. Metzger, P. Chambon, A. D. Widgerow, T.-L. Tuan, et al., *Science* **2017**, *355*, 748.
[37] S. Aarabi, K. A. Bhatt, Y. Shi, J. Paterno, E. I. Chang, S. A. Loh, J. W. Holmes, M. T. Longaker, H. Yee, G. C. Gurtner, *FASEB J.* **2007**, *21*, 3250.
[38] S. Chen, Y. Zhu, Q. Xu, Q. Jiang, D. Chen, T. Chen, X. Xu, Z. Jin, Q. He, *Nat. Commun.* **2022**, *13*, 5684.
[39] Y. Zhang, S. Wang, Y. Yang, S. Zhao, J. You, J. Wang, J. Cai, H. Wang, J. Wang, W. Zhang, J. Yu, C. Han, Y. Zhang, Z. Gu, *Nat. Commun.* **2023**, *14*, 3431.
[40] N. Noskovicova, R. Schuster, S. van Putten, M. Ezzo, A. Koehler, S. Boo, N. M. Coelho, D. Griggs, P. Ruminski, C. A. McCulloch, B. Hinz, *Nat. Biomed. Eng.* **2021**, *5*, 1437.